EUROFUSION WPMST1-PR(16) 15000

L Frassinetti et al.

ELM behavior in ASDEX Upgrade with and without nitrogen seeding

Preprint of Paper to be submitted for publication in Nuclear Fusion

This work has been carried out within the framework of the EUROfusion Consortium and has received funding from the Euratom research and training programme 2014-2018 under grant agreement No 633053. The views and opinions expressed herein do not necessarily reflect those of the European Commission.

ELM behavior in ASDEX Upgrade with and without nitrogen seeding

L. Frassinetti[1], M. G. Dunne[2], M. Beurskens[3], E. Wolfrum[2], A. Bogomolov[4], D. Carralero[2], M. Cavedon[2,5], R. Fischer[2], F. M. Laggner[6], R. M. McDermott[2], H. Meyer[7], G. Tardini[2], E. Viezzer[2], the EUROfusion MST1 Team* and the ASDEX-Upgrade Team[2]

[1]Division of Fusion Plasma Physics, KTH Royal Institute of Technology, Stockholm SE

[2]Max-Planck-Institut für Plasmaphysik, D-85748 Garching,Germany

[3] Max-Planck-Institut für Plasmaphysik, D-17491 Greifswald, Germany

[4]FOM-Institute DIFFER, Dutch Institute for Fundamental Energy Research,
5600 HH Eindhoven, The Netherlands

[5]Physik-Department E28, Technische Universität München, Garching Germany

[6]Institute of Applied Physics, TU Wien, Fusion@ÖAW, 1040 Vienna, Austria

[7]CCFE, Culham Science Centre, Abingdon, Oxon OX14 3DB, UK

Abstract

The Type I ELM behavior in ASDEX Upgrade with full W plasma facing components is studied in terms of time scales and energy losses for a large set of shots characterized by similar operational parameters but different nitrogen seeding rate and input power. ELMs with no nitrogen can have two typical behaviors, that can be classified depending on their duration, the long and the short ELMs.

The work shows that both short and long ELMs have a similar first phase, but the long ELMs are characterized by a second phase with further energy losses. The second phase disappears when nitrogen is seeded with a flux rate above 10^{22}(e/s). The phenomenon is compatible with a threshold effect. The presence of the second phase is related to a high divertor/scrape-off layer (SOL) temperature and/or to a low pedestal temperature.

The ELM energy losses of the two phases are regulated by different mechanisms. The energy losses of the first phase increase with nitrogen which, in turn, produce the increase of the pedestal temperature. So the energy losses of the first phase are regulated by the pedestal top parameters and the increase with nitrogen is due to the decreasing pedestal collisionality. The energy losses of the second phase are related to the divertor/SOL conditions. The long ELMs energy losses increase with increasing divertor temperature and with the number of the expelled filaments.

In terms of the power lost by the plasma, the nitrogen seeding increases the power losses of the short ELMs. The long ELMs have a first phase with power losses comparable to the short ELMs losses. Assuming no major difference in the wetted area, these results suggest that (i) the nitrogen might increase the divertor heat fluxes during the short ELMs and that (ii) the long ELMs, despite the longer time scale, are not beneficial in terms of divertor heat loads.

*see http://www.euro-fusionscipub.org/mst1

1. INTRODUCTION

Edge localized modes (ELMs) [Zohm PPCF1996] are a type of magnetohydrynamic instability that characterize H-mode plasmas. The ELMs are localized near the plasma edge, in the pedestal region, where they produce a sudden collapse of plasma temperature and density profiles with the consequent expulsion of energy and particles from the plasma to the machine wall and the divertor target [Eich PRL2003, Eich PPCF2005, Eich JNM2011, Sieglin PPCF2013]. Multi-machine studies performed on DIII-D, ASDEX, JT60U and JET-C [Loarte PPCF2003] have shown that the ELM energy losses (ΔW_{ELM}) increase with decreasing collisionality. ITER will operate at low collisionality and ELM energy losses $\Delta W_{ELM}/W_{ped}$ up to 15% have been predicted (where W_{ped} is the pedestal stored energy). The heat loads produced by the ELMs might severely damage the divertor. In particular, material studies have shown that the maximum tolerable ELM energy loss in ITER is approximately 1MJ for the baseline Q_{DT}=10 ITER scenario [Zhitlukin JNM2007, Pitts JNM 2011], corresponding to approximately 1% of the ITER pedestal stored energy. It is therefore important to implement and study techniques to actively suppress/mitigate ELMs (for example by applying resonant magnetic perturbations [Evans PRL2004, Kirk NF2015, Suttrop PRL2011, Liang PRL2007]) and/or reduce the ELM heat loads on the divertor. The nitrogen seeding is a common technique to reduce the power load via radiative cooling [Kallenbach PPCF2010, Fuchs JNM2011, Giroud NF2012, Giroud NF2013], but it is mostly efficient in the inter-ELM periods.

To reduce the long term tritium retention, ITER will operate with beryllium in the main chamber and tungsten in the divertor and DEMO is planned to operate with a full tungsten wall. To improve the prediction for ITER and DEMO, ASDEX Upgrade (AUG) operates with a DEMO-relevant full W wall (AUG-W) since approximately 2007 [Neu JNM2007]. For similar reasons, JET has replaced the carbon wall with an ITER-like wall (JET-ILW), composed mostly by Be in the main chamber and by W in the divertor [Matthews JNM2013], since 2010. In a full metal machine, the missing carbon radiator leads to high target temperatures so impurity seeding has become important to protect the divertor, in particular with high power operations [Kallenbach PPCF2010]. The present work describes the effect of nitrogen seeding on ELMs in AUG-W and will discuss a comparison with the JET-ILW results [Frassinetti NF2015].

The first description of the nitrogen effect on Type I ELMs in AUG-W has been presented in [Schneider PPCF2014, Schneider PPCF2015]. The results described in [Schneider

PPCF2014] showed that the ELM crash in AUG-W with no N seeding is characterized by two phases. The first ELM crash phase has a strong broadband magnetic activity and shows the increase of the divertor themo-currents. This is then followed by a phase characterized by a slightly weaker magnetic activity, constant divertor themo-currents but by a further reduction in the stored energy. From the point of view of the thermal profiles, a collapse of electron temperature T_e and electron density n_e in the pedestal region is observed in both phases. However, the first phase tends to affect mainly the pedestal top region, while in the second phase the profile collapse is extended to the entire pedestal region. This was particularly evident in the density, showing that the second phase is characterized mainly by convective energy losses. The results described in [Schneider PPCF2014] shows that nitrogen seeded discharges are characterized by ELMs in which only the first phase is present and by an increase of the ELM frequency, f_{ELM}. A reduction of the ELM energy losses (ΔW_{ELM}) with nitrogen seeding was observed. But, due to the f_{ELM} increase, no reduction of the integrated ELM power losses (defined as $f_{ELM} \times \Delta W_{ELM}$) was estimated. More recently [Schneider PPCF2015], it has been observed that ELMs of all sizes and durations can occurs in the same discharge in AUG-W.

This first characterization of the ELM behavior with and without nitrogen seeding in AUG-W shows similarities and differences with the ELM behavior in JET-ILW [Frassinetti NF2015]. In JET-ILW with no nitrogen seeding, two types of behavior were observed within the same discharge. The initial phase of the ELM crash was observed to be the same for all the events showing similar magnetic activity, similar T_e drops and n_e drops, similar energy losses and similar time scales (1-2ms). After the first phase, a recovery occurred for approximately 40-50% of the ELMs, while, for the remaining ELMs, a further drop in the pedestal T_e and n_e led to larger energy losses. The energy losses were dominated by the convective transport. This second phase was significantly longer (up to 10-15ms) and was dubbed “slow transport event”. Like in AUG-W, nitrogen seeding led to the disappearance of the the second phase. However, in contrast to the AUG-W results, in JET-ILW an increase of the ELM energy losses with N seeding was observed.

The present work extends the results of AUG-W described in [Schneider PPCF2014] and presents a systematic study of the ELM dynamics and energy losses with nitrogen seeding. The work shows that the results so far obtained in AUG-W and in JET-ILW are not in contradiction and that the ELM behavior with/without nitrogen is consistent in both machines. The work also describes the differences between the first and the second ELM phase, showing

that the initial ELM crash is related to the pedestal top parameters, while the second phase is correlated to the scrape-off layer (SOL) and/or the pre-ELM divertor conditions.

The paper is organized as follows. Section 2 describes the short and the long ELMs in AUG-W and how the long ELMs are related to the expulsion of filaments. Section 3 describes the effect of nitrogen on the ELM dynamics, in particular on the presence of the second phase of the ELM and on the ELM energy losses. Section 4 discusses the effect of the nitrogen on the ELM duration and on the ELM power losses. Section 5 shows that the short ELMs are mainly related to the pedestal top parameters, while the long ELMs are related also to the divertor and/or SOL conditions. In Section 6, the experimental results are discussed and a possible physical mechanism responsible for the long ELMs is presented. The conclusions are reported in section 7.

2. SHORT AND LONG ELMS

Earlier works have shown that AUG-W with no nitrogen seeding is characterized by Type I ELMs composed of two phases [Schneider PPCF2014]. The first phase, dubbed as (Ia) in earlier works, is characterized by a quick rise in the divertor current (I_{div}), by a strong high frequency magnetic activity and by a sudden loss of energy and particles. Drops of temperature and density are observed at the pedestal top. The second phase, dubbed (Ib), is characterized by a saturation (or slow increase) in I_{div}, by a slightly weaker high frequency magnetic acitivity and by a further, but weaker, reduction in the stored energy. From the point of view of the kinetic profiles, it has been observed that phase (Ib) corresponds to a collapse of the entire transport barrier..

2.1 TIME EVOLUTION AND TIME SCALE OF THE ELM

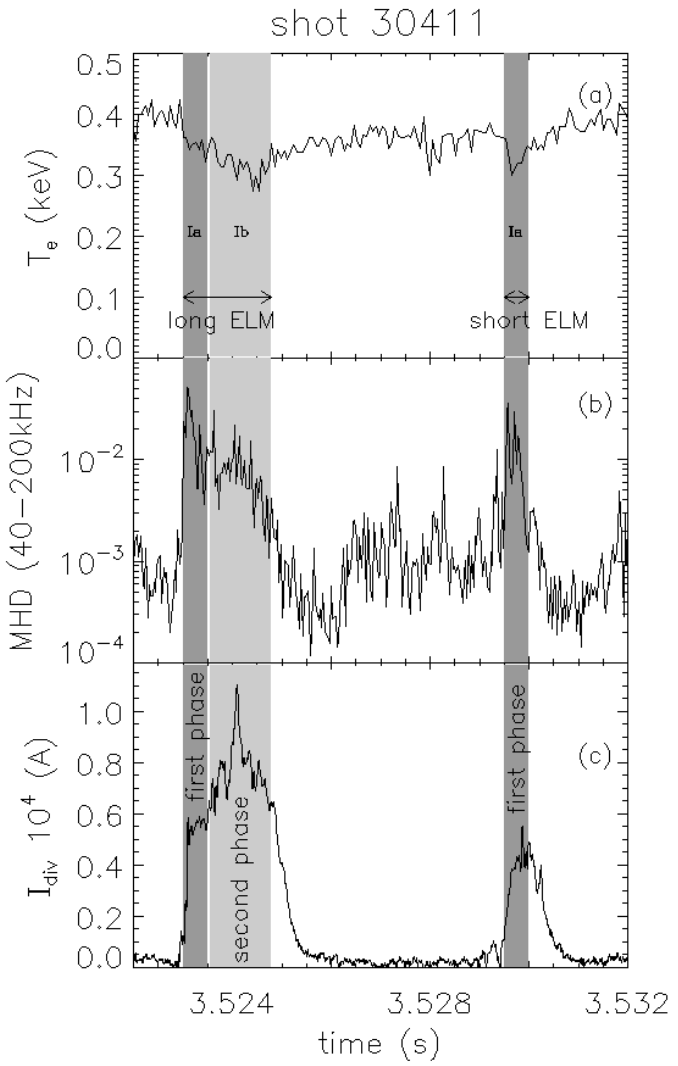

Figure 1. *(a). Time traces of (a) pedestal temperature (b) high frequency magnetic activity from coil B31-14 and (c) divertor current during a stationary phase of shot 30411 with no N seeding.*

The present work extends the previous analysis. It can be observed that in AUG-W with no N seeding it is possible to observe both ELMs with phase (Ia) and (Ib) and ELMs with phase (Ia) only. An example is shown in figure 1. The time trace of the electron temperature at the pedestal top is shown in figure 1(a), the high frequency magnetic acitivity in figure 1(b) and the divertor current in figure 1(c). The magnetic acitivty is measured by a pick up coil which is located at the outboard midplane and measures the radial component of the magnetic perturbations [Maraschek EPS1998]. The high frequency magnetic acitivity has been calculated by integrating the frequency spectrum in the range 40kHz-200kHz. The frequency range has been chosen

above 40kHz to eliminate possible low frequency activities not related to the ELMs. The divertor currents, that are created by thermoelectric effects due to the temperature difference between two scrape-off layer ends [Staebler NF1989], are measured by means of shunts in an outer target tile [Kallenbach JNM2001]. The divertor current is dependent on the divertor temperature and the signal is very sensitive to the ELM dynamics [Schneider PPCF2014]. At t≈3.524s, an ELM characterized by phase (Ia) and (Ib) is shown. The phase (Ia) is characterized by a quick increase in I_{div}, by a peak in the magnetic acivity and by a drop in the pedestal temperature. The phase (Ib) is characterized by a weaker increase in I_{div}, by a lower magnetic activity and by a further reduction in the temperature. On the other hand, at t≈3.530s, another ELM is shown, but only phase (Ia) is present. The duration of this second ELM is clearly shorter than the duration of the first ELM.

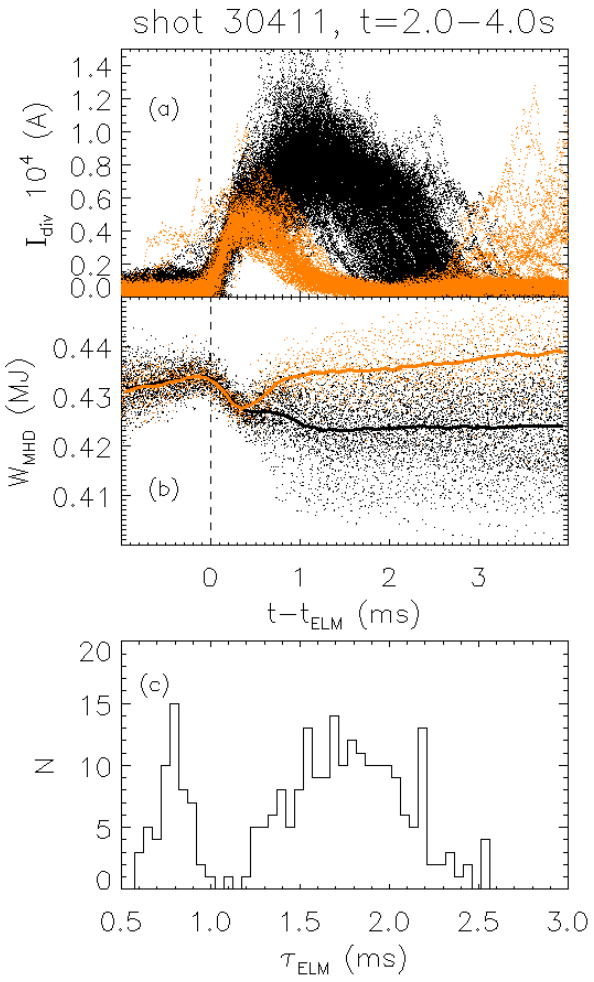

Figure 2. *ELM synchronized time traces of (a) divertor currents and (b) stored energy. (c) histogram of the ELM duration calculated has the FWHM of the divertor current from frame (a). The orange color corresponds to the ELMs with* τ_{ELM}*<1.1ms and the black color to the ELMs with* τ_{ELM} *>1.1ms. The continuous lines in frame (b) highlight the conditional average of the stored energy for short (orange) and long ELMs (black). Data correspond to a stationary phase between t=2-4s at* P_{NBI}*=5MW with no N seeding.*

The presence within the same shot of both long ELMs [characterized by phase (Ia) and (Ib)] and short ELMs [characterized only by phase (Ia)] is common when nitrogen is not seeded. In the shot of figure 1, approximately 20-25% of the ELMs have only phase (Ia). This is shown in detail in figure 2(a), where the I_{div} time traces from t=2s to t=4s have been ELM-synchronized in order to have at t=0 the beginning of the crash for each ELM. The ELMs considered in figure 2 belong to a stationary phase characterized by constant power, gas and confinement and by no N are shown. Two distinct behaviors can be observed: in 20-25% of the ELMs, I_{div} starts to decrease after ≈0.5ms (orange data) while in the remaining ELMs, I_{div} continues to increase till ≈1.0ms. The ELM duration τ_{ELM} has been quantified by

calculating the full width half maximum of I_{div}. The histogram of τ_{ELM} corresponding to the data of figure 2(a) is shown in figure 2(c). Two distinct groups can be observed: (1) the ELMs with τ_{ELM}>1.1ms are those characterized by phases (Ia) and (Ib). (2) the ELMs with τ_{ELM}<1.1ms are those characterized only by phases (Ia).

The separation in τ_{ELM} between these two groups is very clear. This occurs for all the shots in which both long and short ELMs are present. This characteristic has been used throughout the paper to systematically separate ELM with phase (Ia) and (Ib) from ELMs with only phase (Ia). In figure 2(a) and in the rest of the paper, the colors have been chosen according to this criterion: orange for τ_{ELM}<1.1ms and black for τ_{ELM}>1.1ms. Using this criterion of separation, also all other signals show two distinct behaviors. For example, figure 2(b) shows the ELM synchronized W_{MHD}. The first phase of the crash is similar for all ELMs, till t-t_{ELM}≈0.5ms, with ELM energy losses in the range ΔW_{ELM}≈5-7kJ. At t-t_{ELM} >0.5ms, the recovery starts for the ELMs characterized by only phase (Ia), orange color, while the energy losses continue for the ELMs characterized also by phase (Ib), black color, even though with a slightly slower rate. The ELMs with phase (Ib) have ΔW_{ELM}≈12kJ.

This behavior is the same observed in JET-ILW with no N seeding [Frassinetti NF2015], where two disctinct time scales in the ELM crash have been observed and where only the first phase was observed in 30-40% of the ELMs. The time scale of the JET-ILW ELMs characterized by only the first phase was ≈2ms, while the time scale of the JET-ILW ELMs characterized by both the first and the second phase was ≈9ms. However, time scale was estimated from the drop in the pedestal temperature, so the JET-ILW and AUG-W ELM time scales are not directly comparable.

2.2 TERMINOLOGY USED IN THE PAPER

In section 2.1 we have shown that with no nitrogen seeding AUG-W and JET-ILW have the same ELM phenomenology, but slightly different terminology in describing the ELM phases. To avoid confusion, the following terminology will be used in the rest of the paper. Phase (Ia) will be called “first phase”. Phase (Ib), corresponding to the slow transport event in JET-ILW, will be called “second phase”. The ELMs composed by only the first phase will be called “short ELMs”. The ELMs characterized by both the first and second phase will called “long ELMs”. Herefater, when addressing to the properties of the “long ELMs” (for example the ELM energy losses), the entire ELM crash will be considered, i.e. first phase and second phase together. The terms “(Ia), (Ib)” and “slow transport event” will be no longer used.

2.3 SHORT AND LONG ELMS AND FILAMENTS

The long ELMs are characterized by the expulsion of filaments during the second phase. The filanements have been studied using a diagnostic for electron cyclotron emission imaging, ECEI [Classen RSI2010], which covers a 10cm x 40cm area at the outer midplane. The correlation beween ELMs and number of filaments has been investigated in detail in [Bogomolov NF2016]. The filaments have been identified as relatively hot structures (compared to the background).

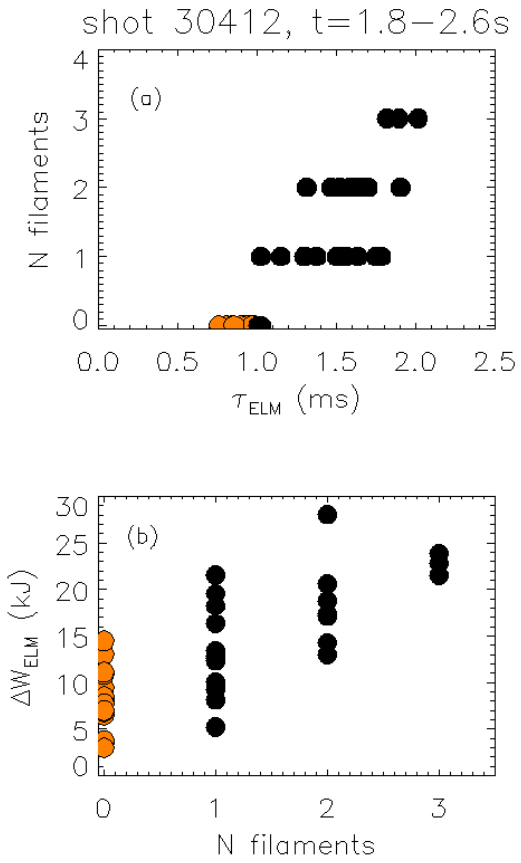

Figure 3. (a) *Correlation between number of expelled filaments and ELM duration and (b) between the ELM energy losses and the number of filaments. The orange data represent the short ELMs, while the black data the long ELMs. Data corresponds to a stationary phase between 1.8-2.6s at P_{NBI}=5MW with no N seeding for shot 30412.*

Figure 3(a) shows the correlation between ELM duration and the number of measured filaments. Due the the ECEI geometry, and taking into account the filament rotation (≈2km/s [Boom NF2011]), the fraction of filaments that can be measured by the diagnostic is approximately ≈24% [Bogomolov NF2016]. Each data point represents one ELM and the color code is consistent with figure 2: the orange data represent the ELMs characterized by only the first phase and the black data represent the ELMs characterized by the first and second phase. No filaments are observed in the short ELMs, while up to three filaments have been observed in the long ELMs. The longer the ELM duration, the more filaments are expelled.

The filaments are a channel of energy losses. This could explain why the long ELMs have higher ΔW_{ELM} than the short ELMs. Indeed, ELM energy losses and number of filaments are reasonably well correlated, as shown in figure 3(b).

The origin of the second phase in the ELM crash is investigated in Section 5.

3. EFFECT OF NITROGEN SEEDING ON LONG AND SHORT ELMS AND ON THE ENERGY LOSSES.

To study in detail the effect of nitrogen seeding on the ELMs, a set of discharges obtained using the same operative parameters but different NBI power and different nitrogen puff rate has been performed. Section 3.1 describes the data set used. Section 3.2 describes the effect of nitrogen seeding on the presence of long and short ELMs and section 3.3 describes the effect of nitrogen on the ELM energy losses.

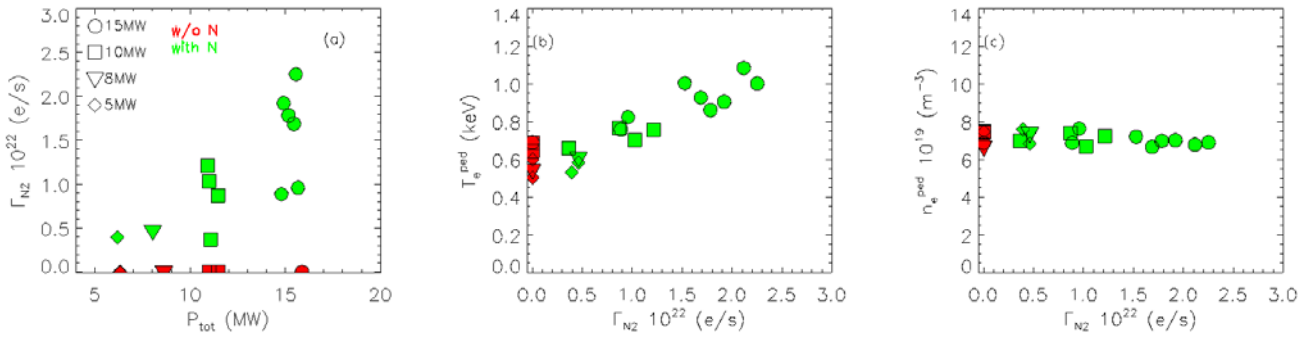

Figure 4. *(a) nitrogen puff rate and total input power (NBI, ECRH and ohmic) for the dataset used in this work. (b) pedestal electron temperature and (c) density versus nitrogen rate. The pedestal values have been estimated from the Thomson scattering profiles calculate at the pedestal top (at ρ_{pol}=0.85). Each data point represents a time average in a stationary interval (each interval at least 0.5s long). The green data highlight the shots with nitrogen and the red data those without. The symbols highlight the NBI power: 5MW (triangles), 8MW (diamonds), 10MW (squares) and 15MW (circles). This color-symbol code is used throughtout the paper.*

3.1 THE DATASET

The dataset is composed of H-mode discharges with I_p=1.0MA, B_t=-2.5T q_{95}=4.2 at low triangularity. The rate of the main gas is kept constant at $\Gamma_D \approx 3 \cdot 10^{22}$(e/s) and the Greenwald fraction is $f_{GW} \approx 0.65$. Excluding the NBI power and the nitrogen puff rate, the operative parameters are the same in the entire dataset. Four NBI power levels have been used, 5MW, 8MW, 10MW and 15MW. At each power level, the nitrogen puff rate Γ_N has been increased in steps from $\Gamma_N \approx 0$ up to just below the level that produces detachment [Kallenbach NF2015, Zohm NF2013]. The detachment would cause a strong increase in the plasma density, affecting the confinement and significantly complicating the interpretation of the results. The nitrogen puff rate necessary to reach detachment is higher at high power and only low levels of nitrogen rate can be applied at low power to avoid detachment. Γ_N and P_{NBI} for the present dataset are shown in figure 4(a). For each discharge, only stationary time intervals have been considered. The stationary time intervals used in this analysis are at least 0.5s long (the energy confinement time is in the range $\tau_E \approx 0.06$-0.1s) and have constant operative parameters (Ip,

q_{95}, shape, Γ_D, Γ_N, P_{NBI}) as well as constant plasma confinement (stored energy and pedestal pressure). Each data point represents the time average during the stationary time interval.

The ELMs studied in this work are Type I. This is supported by the observed increase of the ELM frequency with the power through the separatrix and by the fact that the loss power is well above the L-H threshold power.

The increase of confinement with nitrogen seeding in a metal wall machine is well known both in AUG-W [Schweinzer NF2011, Beurskens PPCF2013, Dunne EPS2015, Dunne APS2015] and in JET-ILW [Giroud NF2013, Giroud PPCF2015]. Before starting to investigate the effect of nitrogen seeding on the ELMs, it is useful to identify the effect of nitrogen seeding on the pedestal pressure. Figure 4(b) and figure 4(c) show the correlation between the pedestal electron temperature and density with the nitrogen puff rate. The pedestal density does not change significantly. On the other hand, a positive correlation (approximately linear) is present between the nitrogen puff rate and the pedestal temperature. A similar trend has been observed for the ion temperature. This confirms that the improved confinement produced by N seeding is related mainly to the temperature increase, as already discussed in [Schweinzer NF2011, Dunne EPS2015].

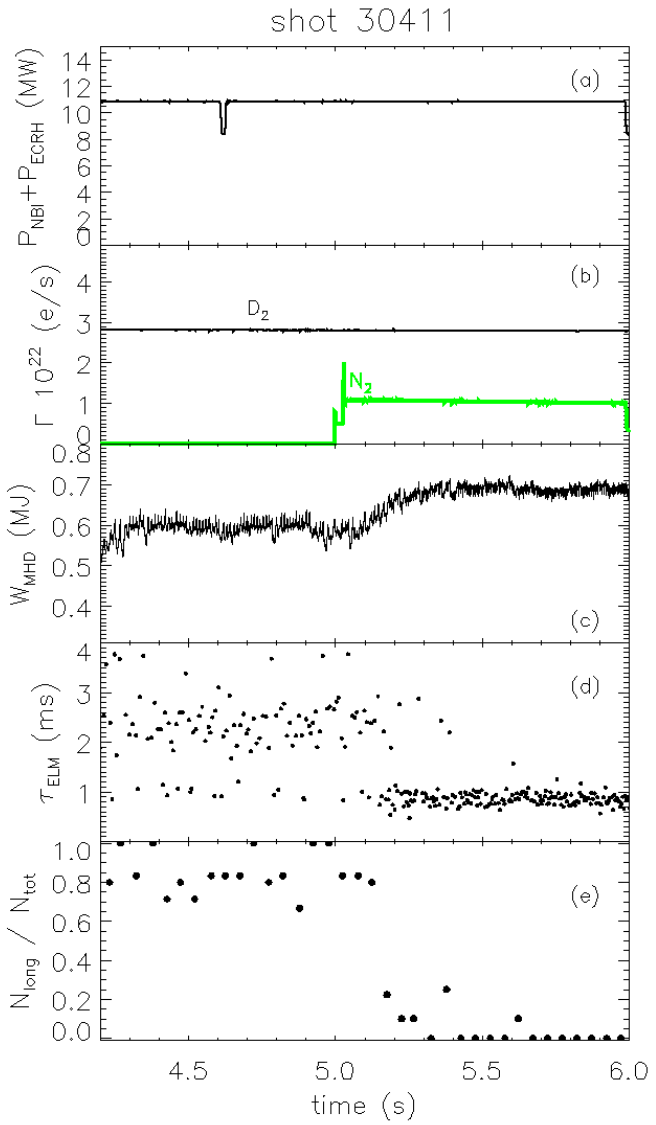

Figure 5. *Time traces of (a) NBI and ECRH power, (b) deuterium flow (black) and nitrogen flow (green), (c) stored energy, (d) ELM duration measured from the divertor current and (e) fraction of long ELMs over the total number of ELMs (calculated from frame (d) by binning the data in 50ms long intervals).*

3.2 LONG AND SHORT ELMS WITH NITROGEN SEEDING

The effect of nitrogen seeding on the presence of the long ELMs is shown in figure 5 for shot 30411. The total power and the flow of the main gas are shown in figures 5(a) and 5(b). No nitrogen is seeded till 5s. The stored energy is $W_{MHD}\approx0.6$MJ till $t\approx5$s, figure 5(c). The duration of each single ELM measured from the divertor current is shown in figure 5(d). A behavior similar to that observed in figure 2 is present, with a separation between ELMs with only the first phase (short ELMs, with $\tau_{ELM}<1.1$ms) and ELMs characterized by both the first and the second phase (long ELMs, with $\tau_{ELM}>1.1$ms). Figure 5(e) shows N_{long}/N_{tot}, i.e. the fraction of the number of long ELMs over the total number of ELMs. N_{long}/N_{tot} is approximately 0.8 till 5s, showing that approximately 80% of the ELMs are characterized by both the first and the second phase when nitrogen is not seeded.

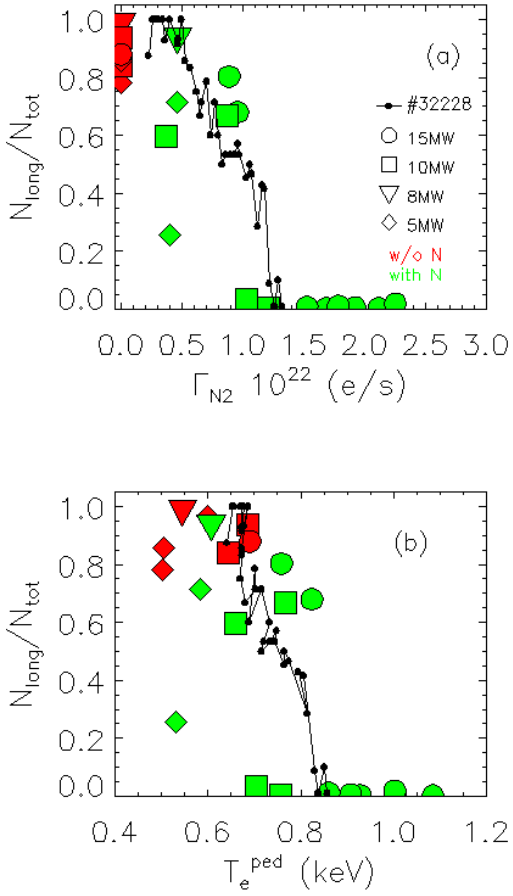

Figure 6. *Number of long ELMs relative to the total number of ELMs versus the nitrogen rate (a) and (b) versus the pedestal temperature. The same dataset of figure 4 is used. The black data shows the result from a gas ramp shot (from figure 7.*

Nitrogen is then seeded from t=5.0s while keeping the other operative parameters constant. In the shot of figure 5, the nitrogen seeding produces an increase in the stored energy from $W_{MHD}\approx0.6$MJ to $W_{MHD}\approx0.7$MJ. The effect of nitrogen on the ELMs is shown in figures 5(d) and 5(e). When nitrogen is seeded, the second phase of the ELMs disappears and only short ELMs, with $\tau_{ELM}<1.1$ms, remain present.

The reduction of N_{long}/N_{tot} with the increasing nitrogen does not seem gradual and data seem to suggest a threshold at $\Gamma_N\approx10^{22}$(e/s). This can be observed in figure 6(a), where the correlation between N_{long}/N_{tot} and Γ_N is shown for the entire dataset. In this figure, each data point represents a time average during a stationary phase. With no nitrogen (red data), approximately 80-100% of the ELMs have the second phase. Once the nitrogen puff rate is increased to $\Gamma_N\approx10^{22}$(e/s), the fraction of long ELMs tends to decrease to 60-80%. For higher nitrogen puff rates, no long ELMs are observed.

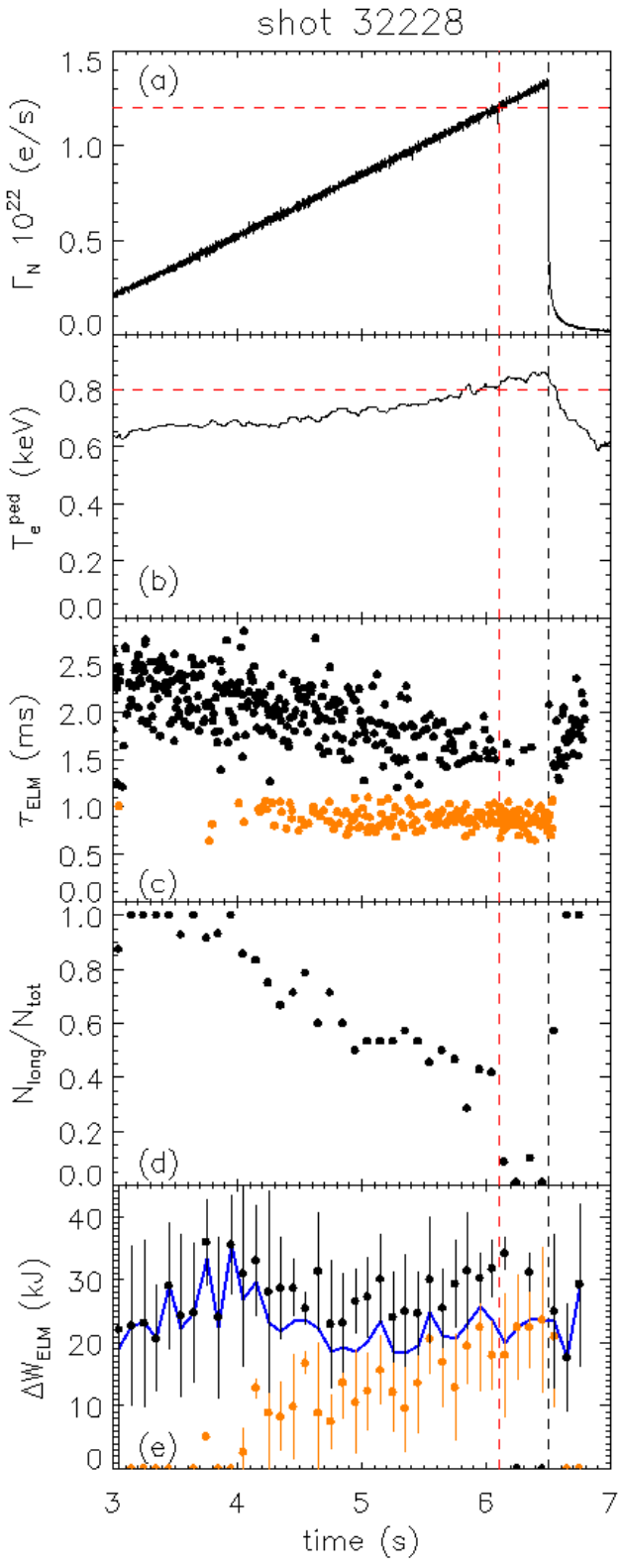

Figure 7. *Time evolution of (a) nitrogen puff rate, (b) pedestal temperature, (c) ELM duration, (d) N_{long}/N_{tot}, and (e) ELM energy losses for shot 32228 (P_{NBI}=10MW). In frames (c) and (e), long ELMs are in black and short ELMs in orange. The red veritical line highlights the time at which N_{long}/N_{tot} drops. The vertical black line highlights the time at which nitrogen flow is tuned off. The blue line in frame (e) highlights the energy losses calculated without separating long and short ELMs. Results in frames (d) and (e) have been calculated by binning the data in 100ms long intervals.*

From a physicsl point of view, it is useful to verify if the disappearance of the long ELMs is related to the pedestal top parameters. In figure 6(b), the correlation between N_{long}/N_{tot} with the pedestal temperature T_e^{ped} is shown. Due to the fact that Γ_N and T_e^{ped} are strongly correlated [figure 4(c)], the message is essentially similar to that of figure 6(a): no gradual reduction of N_{long}/N_{tot} is observed with increasing temperature and for T_e^{ped} >0.8keV long ELMs are not present. On the contrary, between T_e^{ped}≈0.65-0.85keV both mainly long or mainly short ELMs can be observed. It is essential to highlight that figure 6(b) does not imply that the pedestal temperature is the plasma parameter that regulates the presence of the long ELMs. Any parameter related to the pedestal temperature, such as pressure, stored energy, collisionality or resistivity, would show a similar trend.

To further investigate if the disappearance of the long ELMs is related to a threshold effect, figure 7 shows a shot with constant operative parameters but with a ramp in the nitrogen puff rate, figure 7(a). The pedestal temperature steadily increases with the nitrogen, figure 7(b). The ELM duration is shown in figure 7(c).

The duration of the long ELMs (in black) tends to decrease with increasing nitrogen. The fraction of long ELMs over the total ELMs is shown in figure 7(d). The results show a steady reduction of N_{long}/N_{tot} with increasing nitrogen (and temperature) till t≈6.1s at $\Gamma_N \approx 1.2 \cdot 10^{22}$(e/s) and $T_e^{ped} \approx 0.8$keV. At higher rates of nitrogen, a sudden reduction from $N_{long}/N_{tot} \approx 0.4$ to $N_{long}/N_{tot} < 0.1$ is observed. So, the data of figure 7 are consistent with a gradual reduction of the long ELMs combined with a threshold effect. However, we must highlight that the shot is not in stationary conditions, so a firm conclusion is not possible. Note that the long ELMs reappear soon after the nitrogen flow is closed. For comparison with the dataset of section 3.1, the correlations of N_{long}/N_{tot} versus Γ_N and versus T_e^{ped} for the nitrogen ramp shot is shown in figure 6 as (black data). A reasonable agreement is present between the data of the nitrogen ramp shot and the data of the dataset obtained in stationary conditions.

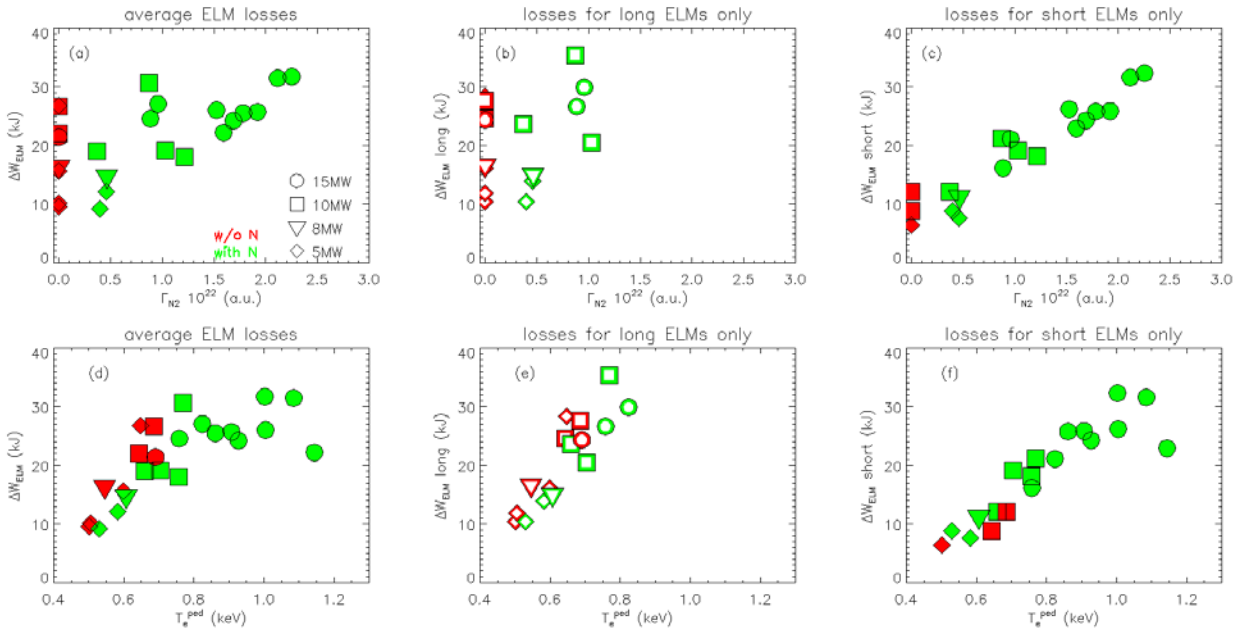

Figure 8. *Energy losses versus the nitrogen rate (top row) and the pedestal temperature (bottom row). The first column shows the average ELM energy losses without separating between long and short ELMs. The second column shows the energy losses for the long ELMs. The third column shows the energy losses for the short ELMs. The same dataset of figure 4 is used.*

3.3 ELM ENERGY LOSSES WITH NITROGEN SEEDING

Earlier results have shown that the nitrogen seeding can affect the ELM energy losses both in AUG-W [Schneider PPCF2014] and in JET-ILW [Frassinetti NF2015]. However, the conclusions were opposite in the two machines. While in AUG-W a reduction of the ELM energy losses was observed with nitrogen seeding, in JET-ILW an increase was observed. This section shows that both results are correct and that the two statement are not in

contradiction as long as the energy losses for long and for short ELMs are considered separately.

The ELM energy losses (ΔW_{ELM}) have been calculated from W_{MHD} as the difference between the pre-ELM stored energy and the minimum stored energy after the ELM. The ELM energy losses for the nitrogen ramp shot are shown in figure 7(e). Each data point is the average of the energy losses of the ELMs located in 100ms long time intervals. The energy losses calculated without separating long and short ELMs (blue continuous line) show a reduction from t=4s, when the fraction of long ELMs starts to decrease, till t=5s, after which a constant value is reached. This reduction is consistent with the results described in [Schneider PPCF2014] were the decrase of the ELM energy losses with nitrogen seeding was observed. Then, the energy losses have been calculated separately for the long ELMs and for the short ELMs, black and orange data respectively. No clear trend is observed for the long ELMs. Instead, an increase of the short ELM energy losses with increasing nitrogen is observed.

To extend the analysis, figure 8 shows the energy losses calculated for the dataset of section 3.1. ΔW_{ELM} has been calculated for each single ELM and then averaged during a stationary phase. Figure 8(a) shows ΔW_{ELM} versus Γ_N. Each data point represents the average during a stationary phase. For a comparative discussion with the earlier AUG-W results, no distinction between long and short ELMs is done yet. No strong correlation between the energy losses and the nitrogen can be observed, however three behaviors can be identified. (I) For $\Gamma_N<10^{22}$e/s, a weak positive trend between ΔW_{ELM} and the nitrogen is present. (II) At $\Gamma_N\approx10^{22}$e/s a reduction of the ELM energy losses can be observed, from $\Delta W_{ELM}\approx$25-30kJ to $\Delta W_{ELM}\approx$18-20kJ. This reduction in the ELM energy losses is basically what is described in [Schneider PPCF2014]. (III) For $\Gamma_N>10^{22}$e/s, a weak positive trend is present. The ELM energy losses (with no disctinction beween long and short ELMs) versus the pedestal tempetature are shown in figure 8(d). ΔW_{ELM} tends to increase with increasing pedestal temperature till $T_e^{ped}\approx$0.8keV. For $T_e^{ped}>$0.8keV, no clear increase of ΔW_{ELM} can be observed.

The time evolution of the stored energy after the first phase of the ELM crash is significantly different between long and short ELM, see figure 2(b). The first phase is similar for all ELMs, but the long ELMs are characterized by a further reduction of the stored energy. Therefore, a detailed investigation of the nitrogen effect on the ELM energy losses requires to separate the losses produced by the long ELMs from those produced by the short ELMs.

Figure 8(b) shows ΔW_{ELM} versus Γ_N for the same dataset of figure 8(a), but considering only the long ELMs. A very weak positive trend can be observed for $\Gamma_N<10^{22}$e/s. For $\Gamma_N>10^{22}$e/s, long ELMs are not present. Figure 8(c) shows ΔW_{ELM} versus Γ_N for the same dataset of figure 8(a), but considering only the short ELMs. A clear positive trend can be observed, with $\Delta W_{ELM}\approx$10kJ with no nitrogen up to $\Delta W_{ELM}\approx$30kJ with maximum nitrogen and maximum power. This is consistent with the result described in JET-ILW [Frassinetti NF2015], where the increase of the ELM energy losses with nitrogen seeding was observed. The ELM energy losses versus the pedestal temperature are shown in figure 8(e) for the long ELMs and in figure 8(f) for the short ELMs. In both cases a positive trend is present.

The results of figure 8 show that it is vital for understanding the ELM physics to separate the behavior of the long ELMs from that of the short ELMs. In fact, the reduction in ΔW_{ELM} at $\Gamma_N\approx10^{22}$e/s observed in figure 8(a) and the saturation of ΔW_{ELM} for $T_e^{ped}>0.8$keV observed in figure 8(d) are due to the disappearence of the long ELMs and not to a general reduction of the ELM energy losses with increasing nitrogen. Basically, the nitrogen can have both (i) a beneficial and (ii) a detrimental effect with respect to the ELM energy losses.

(i) The beneficial effect is related to the disappereance of the second phase of the ELM (which is related to further drops in the stored energy). The investigation on the origin of this phenomenon is presented in section 5.

(ii) The detrimental effect is related to the increase of the energy losses for the short ELMs. This effect can be explained by observing that the nitrogen is well correlated with pedestal temperature and hence with the pedestal collisionality. Figure 9 shows the trend of the ELM energy losses relative to the pedestal stored energy W_{ped} versus the neoclassical pedestal electron collisionality $\nu_e^*(neo)$. The pedestal stored energy has been calculated from the pedestal pressure assuming, for simplicity, $T_i=T_e$ and calculating the ion density from the electron density using Z_{eff} and applying the same method described in [Beurskens NF2013]. The collisionality has been calculated as:

$$\nu_e^*(neo) = qR^{5/2}a^{-3/2}(\lambda_{ee})^{-1}$$

where $\lambda_{ee}=1.7\times10^{17}\ T_e^2(eV)\ /\ [n_e(m^{-3})\ \ln\Lambda]$ is the electron-electron Coulomb collision mean free path, with the temperature and density calculated at the pedestal top [Loarte PPCF2003]. In figure 9, the green and red full symbols represents the relative energy losses of the short ELMs for the present dataset. The increase of the relative energy losses with decreasing collisionality can be observed and the match

with earlier results (the grey full symbols from the multi-machine study discussed in [Loarte PPCF2003]) is reasonable. This suggests that the increase of the energy losses in the short ELMs with increasing nitrogen rate is related to the decrease in collisionality. Several models have been devoleped in literature to explain the correlation of the ELM energy losses with the collisionality. A possibility is that the lower ν_e^* produces the decrease of the mode numbers of the most unstable peeling-modes via the increase of the edge bootstrap current [Loarte PPCF2002]. This can increase the mode spatial structure [Wilson EPS2001] and/or increase the mode growth rate [Becoulet PPCF2001, Becoulet PPCF2003, Pamela PPCF2011] which, in turn, can increase the energy losses.

Figure 9 shows, for comparison, also the energy losses of the long ELMs (green and red empty symbols). An increase of the losses with the decreasing collisionality is observed for the long ELMs as well. However, the long ELMs are composed of a first phase (identical to that of the short ELMs) and a second phase. So, simply, this trend can be ascribed to the scaling of the first phase of the long ELMs with the collisionality.

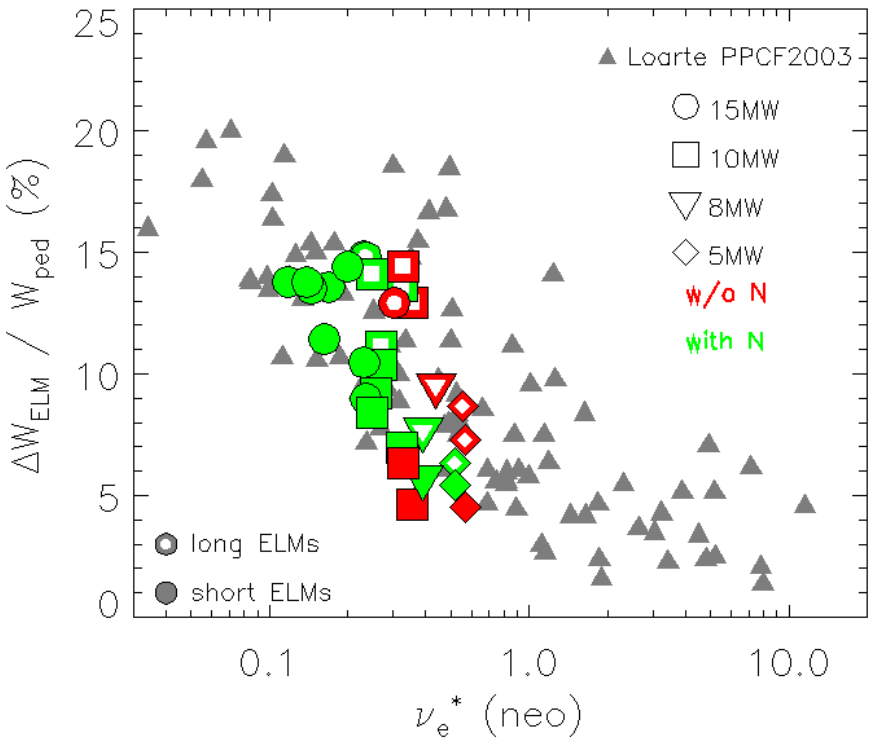

Figure 9. *ELM energy losses relative to the pedestal stored energy versus the neoclassical electron collisionality. Green and red data corresponds to the present AUG-W dataset. The grey data correspond to the multi-machine analysis discussed in [Loarte PPCF2003]*

4. POWER LOST DURING THE ELM WITH AND WITHOUT NIROGEN SEEDING

In ITER and in future fusion reactors, the main problems related to the ELMs are the high heat fluxes that can reach the divertor and damage the target material. A clear measurement of the heat flux with IR cameras is unfortunately not possible for the present dataset. The high divertor density with nitrogen seeding causes high bremsstrahlung radiation, therefore significantly complicating the measurements.

However, a simple, qualitative estimation of the power lost by the plasma during the ELM process can be obtained from the ratio between the ELM energy losses and the ELM duration. This section uses this method to compare the power losses with and without nitrogen seeding for short and long ELMs. The change in the wetted area cannot be estimated, so the power losses might not be directly correlated to the heat flux at the divertor.

4.1 ELM DURATION WITH AND WITHOUT NITROGEN

The ELM duration τ_{ELM} is estimated from the divertor current as described in section 2. The divertor current is used because of its high time resolution and because of its clear correlation with the time scale of the energy losses (see figure 2). τ_{ELM} has been calculated for the same dataset shown in figure 4 separating the short ELMs from the long ELMs. The correlation between τ_{ELM} and the nitrogen puff rate is shown in figure 10(a). A decreasing trend with increasing nitrogen can be observed both for the short ELMs (full symbols) and for the long ELMs (empty symbols). A similar trend can be observed with the pedestal temperature. Concerning the collisionality, figure 10(b), the increase of the ELM duration with increasing collisionality is present. Qualitatively a similar trend with JET-ILW is observed [Frassinetti NF2015].

This result, combined with the increase of the energy losses with nitrogen, suggests that the nitrogen seeding produces the increases of the ELM power losses.

4.2 ELM POWER LOSSES WITH AND WITHOUT NITROGEN

The ELM power losses estimated as the ratio between the ELM energy losses and the ELM duration are shown versus the nitrogen rate in figure 10(c) and versus the pedestal collisionality in figure 10(d). We must highlight that this value is not the power that reaches the divertor but it should be approximately proportional to it. Moreover, this value gives an estimation of the average power lost by the plasma during the entire ELM process. This value

is close to the peak power when considering the short ELMs, but it is lower then the peak power when considering the long ELMs. In the case of long ELMs, in fact, this estimation represents the lost power averaged over the first and second phase together.

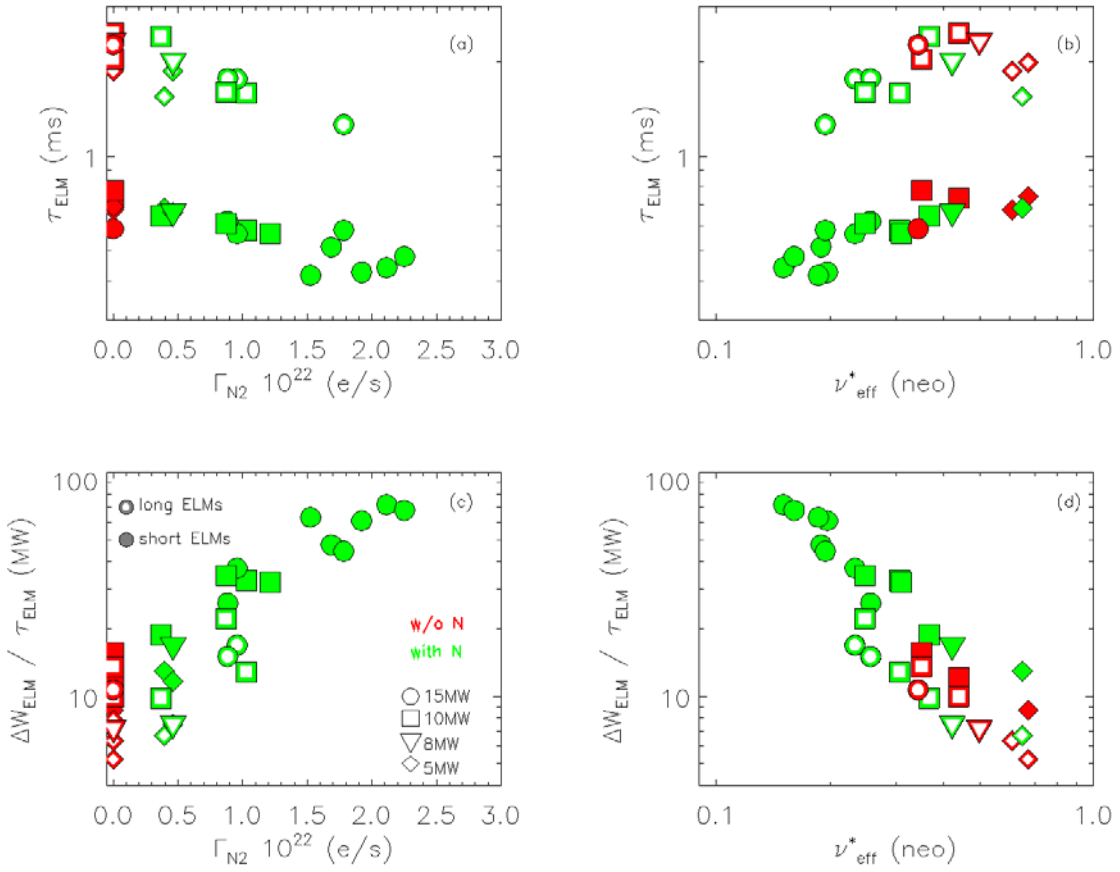

Figure 10. *ELM duration measured from the divertor current versus (a) the nitrogen rate and (b) the pedestal electron collisionality. ELM power losses estimated as the ratio between the energy losses and the ELM duration versus (c) the nitrogen flow and (d)the pedestal electron collisionality.*

The comparison of the power losses between long and short ELMs is shown in figure 10(c) and 10(d). At similar nitrogen rates (or collisionality), compared to the short ELM, the long ELMs tend to have lower average power losses, despite the larger energy losses. This is due to the longer ELM duration.

This observation does not imply that it is favourable to have long ELMs in order to reduce the heat flux on the divertor. In terms of energy losses, the first phase of long ELMs is the same as the short ELMs, so the peak of the power losses is supposed to be the same. This is shown in figure 11, where the time derivative of W_{MHD} is shown for both long and short ELMs. The same data of figure 2(b) have been used. The peak in $d(W_{MHD})/dt$ is the same in both short and long ELMs, approximately 20MW. Assuming that the wetted area is similar in long and short ELMs, the long ELMs are not beneficial for the divertor.

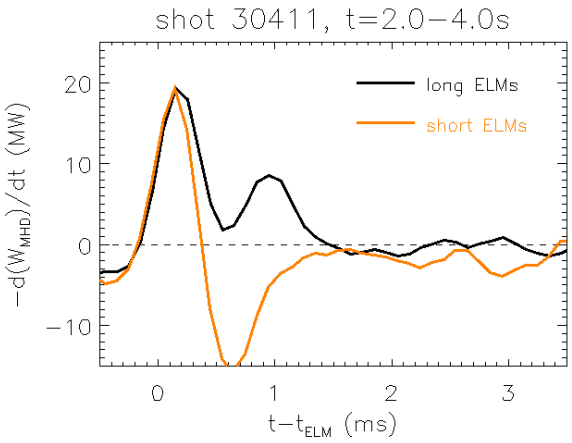

Figure 11. *ELM synchronized time derivative of the stored energy. For the stored energy, the same data of figure 2(b) have been used . The data corresponds to a stationary phase between 2.0-4.0s at P_{NBI}=5MW with no nitrogen seeding for shot 30411.*

Concerning the behavior of the power losses of the short ELMs, figures 10(c) and 10(d) show a clear increase of the power losses with increasing nitrogen and with decrasing collisionality. The power losses increase by a factor 4-5, from ≈10-20MW with no nitrogen to ≈70-80MW with the maximum nitrogen rate. This might suggest that the nitrogen seeding is not efficient for the reducing the ELM heat flux on the divertor. However, we have to highlight two important factors that can attenuate this claim. (I) First of all, the increase by a factor 4-5 is not only due to the increase in the nitrogen, but also due to the increase in the input power [the highest nitrogen rates are obtained with highest input power, see figure 4(a)]. (II) An increase of the power lost by the plasma does not automatically imply an increase of the heat flux on the target. The nitrogen has a radiative cooling effect in the divertor region [Kallenbach PPCF2010, Kallenbach NF2015] that might partially compensates the increase of the power losses.

4.3 INTEGRATED ELM POWER LOSSES WITH AND WITHOUT NITROGEN

From the point of view of the plasma confinement and heating, a useful parameter to study the effect of nitrogen on ELMs is the integrated ELM power loss, defined as $\Delta W_{ELM} \times f_{ELM}$. The integrated ELM power losses give information on the contribution of the ELM to the power balance. In particular it is useful to investigate if the integrated ELM power loss decreases with increasing N.

The integrated ELM power losses have been calculated for shot 32228 in which the nitrogen rate is increased steadily (same shot as figure 7). The corresponding ELM frequency is shown in figure 12(b). The ELM frequency has been calculated as the number of ELMs in a specific time interval divided by the duration of the time interval. Considering both long and short ELMs (blue continuous line), no variation of the ELM frequency with increasing nitrogen is observed. On the other hand, the frequency of the long ELMs (black data) tends decrease with increase nitrogen rate from f_{ELM}≈130-140Hz to f_{ELM}≈50Hz till t≈6.1s Then, f_{ELM} for long ELMs drops quickly and very few long ELMs are observed. The frequency of

the short ELMs (orange data) increases with increase nitrogen rate up to f_{ELM}≈150Hz. The integrated power losses are shown in figure 12(c) and are calculated using the ELM energy

losses from figure 7(e) and the ELM frequency from figure 12(b). Concerning the long ELMs, a reduction of $\Delta W_{ELM} \times f_{ELM}$ is observed with increasing nitrogen rate. This is mainly due to the decrase in the frequency of the long ELMs. Concerning the short ELMs, a marked increase of $\Delta W_{ELM} \times f_{ELM}$ with increasing nitrogen rate is observed. This is due to both the increase in the energy losses and the increase in the ELM frequency. Note that the integrated power losses with the lowest nitrogen rate (only long ELMs present) are comparable to the power losses with the highest nitrogen rate (only short ELMs present). Moreover, the positive trend for short ELMs between $\Delta W_{ELM} \times f_{ELM}$ and nitrogen suggests that even higher integrated power losses can be reached. The integrated power losses calculated without separating long and short ELMs is shown in frame (c) with the blue continuous line. A weak reduction from ≈3.5MW (when no short ELMs are present) to ≈3MW (when no long ELMs are present) can be observed. This result suggests that the nitrogen does not reduce significantly the integrated power losses.

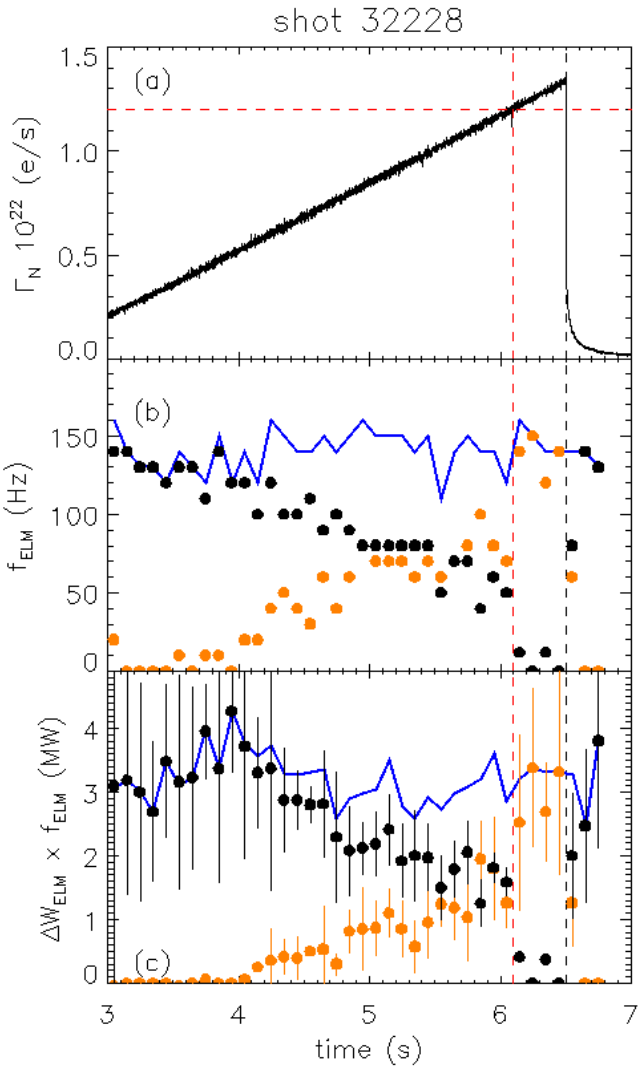

Figure 12. *Time evolution of (a) nitrogen puff rate, (b) ELM frequency and (c) integrated ELM power losses for shot 32228 (P_{NBI}=10MW). In frames (b) and (c), long ELMs are in black and short ELMs in orange. The blue lines highlights fELM and integrated power losses calculated without separating long and short ELMs. The red veritical line highlights the time at which N_{long}/N_{tot} drops. The vertical black line highlights the time at which nitrogen flow is tuned off. Results in frames (b) and (c) have been calculated by binning the data in 100ms long intervals.*

To extend the results, the ELM frequency and the integrated power losses are calculated for the dataset of section 3.1. The ELM frequency is shown in figures 13(a)-(c). A weak increase with increasing nitrogen is observed when all ELMs are considered, figure 13(a). The

ELM frequency of the long ELMs shows a weak reduction with increasing nitrogen, figure 13(b). For example, the 10MW shots have a reduction from 100-130Hz to 70-80Hz before completely disappearing at $\Gamma_N>10^{22}$e/s. The ELM frequency of the short ELMs shows a clear increase with increasing nitrogen, figure 13(c), from ≈50Hz at $\Gamma_N<10^{22}$e/s to 200Hz at $\Gamma_N>10^{22}$e/s. The corresponding integrated ELM power losses are shown in figure 13(d)-(f). Figure 13(d) shows $\Delta W_{ELM} \times f_{ELM}$ calculated without separating long and short ELMs. Comparing the reference cases with no nitrogen with the cases with low nitrogen rate ($\Gamma_N \approx 0.5 \cdot 10^{22}$e/s), a weak reduction is observed from 1-4MW to 1-2MW. Instead, for higher nitrogen rates ($\Gamma_N>0.5 \cdot 10^{22}$e/s), the integrated power losses can be higher with nitrogen than without nitrogen. This behavior is due to two effects:

(i) The integrated power losses of long ELMs tend to decrease when nitrogen is seeded, figure 13(e) and 12(c).

(ii) The integrated power losses of short ELMs increases steadily with nitrogen, figure 13(f) and 12(c) and are very low at low nitrogen rate.

So, at $\Gamma_N \approx 0.5 \cdot 10^{22}$e/s the integrated power losses are slightly reduced for long ELMs and are very small for short ELMs. As a result, considering all the ELMs, a reduction in $\Delta W_{ELM} \times f_{ELM}$ is observed. For $\Gamma_N>0.5 \cdot 10^{22}$e/s the power losses of short ELMs increase with nitrogen. As a result, $\Delta W_{ELM} \times f_{ELM}$ can reach values higher with nitrogen than without.

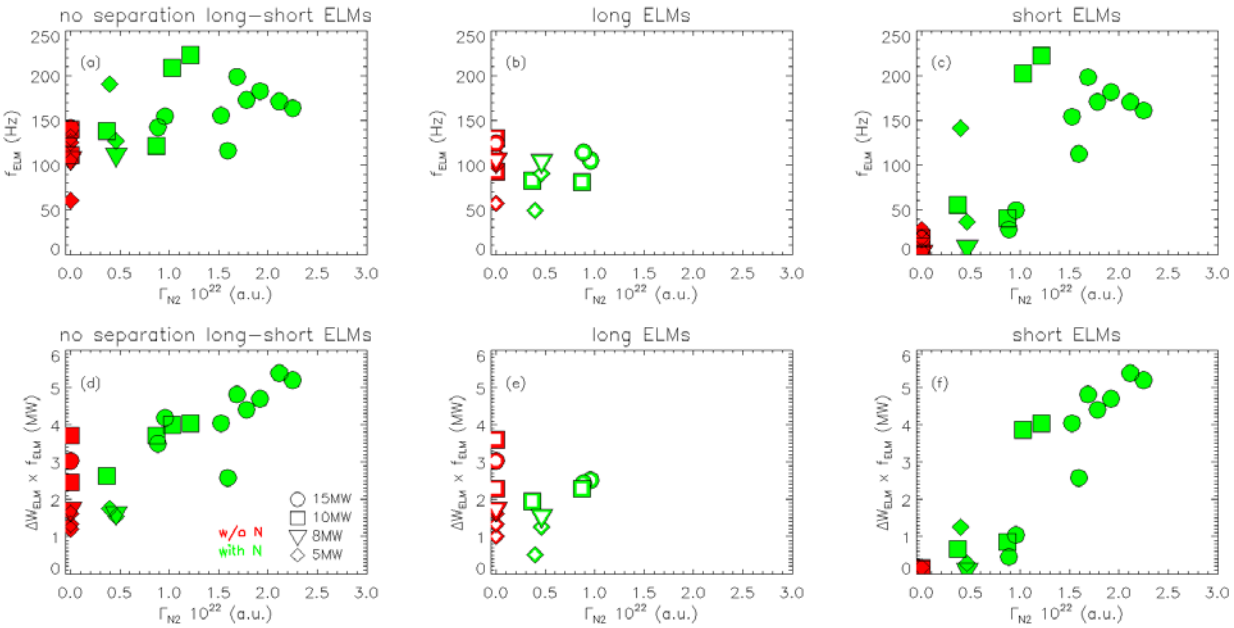

Figure 13. *ELM frequency considering all the ELMs (a), only the long ELMs (b) and only the short ELMs(c) versus the nitrogen puff rate. Integrated ELM power losses considering all the ELMs (d), only the long ELMs (e) and only the short ELMs (f) versus the nitrogen puff rate.*

5. PRE-ELM DIVERTOR TEMPERATURE AND LONG ELMS

This section investigates the origin of the long ELMs and in particular if specific pre-ELM parameters can trigger the long ELMs. The analysis has been performed for the entire dataset described in section 3.1 by calculating the pre-ELM parameters separately for short ELMs and for long ELMs. Within the experimental uncertainty, the results show that no difference between short and long ELMs is present in the pre-ELM parameters at the pedestal top. The parameters that have been considered are electron temperature and electron density measured by the Thomson scattering and the ion temperature measured by the charge exchange. The results discussed in [Schneider PPCF2015] suggests that the presence of long ELMs is not regulated by the pedestal top parameters but might be related to the divertor and or SOL conditions. Figure 14 discusses the correlation of the pre-ELM divertor temperature with the long ELMs.

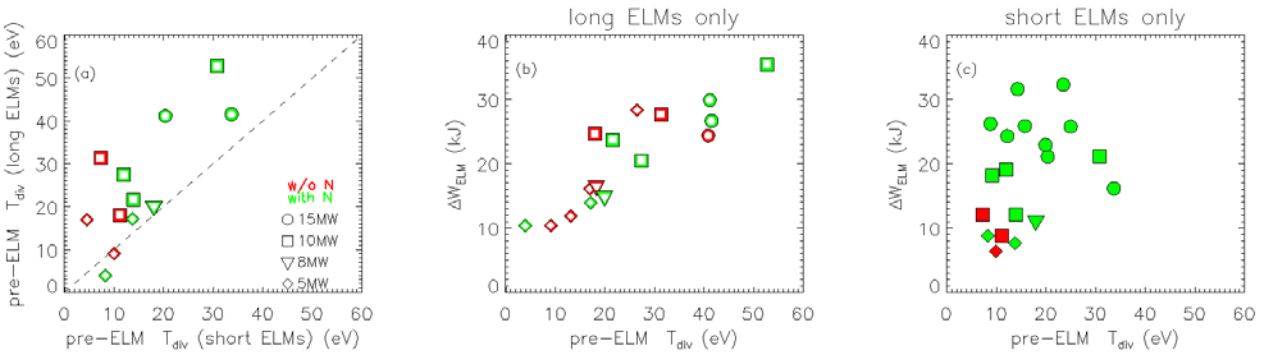

Figure 14. *(a) log ELMs pre-ELM T_{div} versus short ELMs pre-ELM T_{div}. Only stationary intervals characterized by the the presence of both long and short ELMs are considered. (b) ELM energy losses of long ELMs versus the corresponding pre-ELM T_{div}. (c) ELM energy losses of short ELMs versus the corresponding pre-ELM T_{div}.*

The divertor temperature T_{div} has been evaluated from the thermo-electric currents into a divertor tile as described in references [Kallenbach PPCF2010, Kallenbach JNM2001]. The divertor temperature has been time averaged in an interval from -0.6ms to -0.1ms before the ELM. Figure 14(a) shows the pre-ELM T_{div} for the long ELMs versus the the pre-ELM T_{div} for the short ELMs. Each data point represents the average over a stationary interval, as described in section 3. In figure 14(a), only stationary intervals in which both the long and the short ELMs are present have been considered. On average, the long ELMs tend to have pre-ELM divertor temperature higher than the short ELMs.

The correlation between divertor temperature and long ELMs is strengthened in figure 14(b) where the ELM energy losses of the long ELMs versus the corresponding pre-ELM T_{div} is shown. The positive correlation shown in figure 14(b) suggests that the pre-ELM divertor temperature plays an important role not only in triggering the long ELMs, but also in influencing the long ELM energy losses. On the contrary, no clear correlation between the energy losses and the pre-ELM T_{div} is observed for the short ELMs, as shown in figure 14(c). Since the first phase of the long ELMs is similar to the short ELMs, the results of figures 14(b) and 14(c) suggests that the physics mechanism that regulates the energy losses of the second phase is different from the mechanism that regulates the losses of the first phase. A discussion, including comments on possible mechanisms related to the second ELM phase is presented in Section 6.

6. DISCUSSION

This work has discussed the difference between the long and the short ELMs. The origin of the long ELMs is not clear yet. However, the presence of the long ELMs cannot be ascribed to the presence of the metal wall in AUG-W. It was shown in reference [Schneider PPCF2015] that the ELM energy loss and the ELM duration do not show a significant difference between the carbon wall and the metal wall when the pedestal pressure, as well as the separatix density, is the same.

The nitrogen seems to have a major role in the disappearance of the long ELMs. But we can exclude a direct role of the nitogen in the mechanism that regulates the presence of the long ELMs. For example, the JET-ILW experimental results suggest that the long ELMs are not present if the pedestal pressure is sufficiently high, even without nitrogen seeding [Sieglin PPCF2014]. Moreover, it has been observed that the CD_4 seeding produces the same effects on the ELMs as the nitrogen [Beurskens EPS2015, Beurskens NF2016]. Likely, the nitrogen affects the ELMs indirectly by improving the pedestal confinement and/or affecting the divertor/SOL conditions. As shown in figures 4(b), both the pedestal temperature and the pedestal pressure increase with increasing nitrogen. However, with the present dataset it is not possible to clearly identify the parameter that regulates the presence of the long ELMs. We cannot exclude any parameter related to the pedestal temperature, such as collisionality or resistivity. A more clear answer might be obtained by seeding different species, in oder to affect only the pedestal density and not the temperature. This is planned for the future.

Moreover, the results of section 5 suggest that the divertor conditions can affect the long ELMs as well. In particular, it was investigated why, during a stationary condition of the

same shot, a long ELM can be followed by a short ELM. No major difference in the pre-ELM pedestal parameters has been observed between long and short ELMs, while the difference has been observed in the pre-ELM divertor temperature. Within the same shot, the long ELMs tend to have higher pre-ELM T_{div} than the short ELMs. Moreover, while the energy losses of the long ELMs seem to be related to the pre-ELM T_{div}, no correlation is observed for the short ELMs. While the energy losses of the first phase are regulated by the pedestal collisionality, as discussed in section 3.3, the energy losses of the second phase seem to be related to the divertor and/or SOL conditions. This suggests that the physical mechanism that drives the transport in the second phase of the long ELMs is not the same as in the first ELM phase. Higher T_{div} might influence the SOL temperature, T_{SOL}. JOREK simulations [Pamela EPS2014] applied to MAST suggest that the T_{SOL} can influence the ELM energy losses. By varying the T_{SOL} in the range 6eV-25eV, the simulations have shown that the increase of T_{SOL} can (a) increase the ballooning growth rate (b) induce the expulsion of more filaments and (c) extend the perturbation of the ballooning mode much further inside the separatrix. All these effects tend to increase the energy losses. It is not possible to experimentally verify effect (a). Concerning effect (b), figure 3(b) indeed suggests a correlation between the energy losses of the second phase and the number of expelled filaments. Concerning effect (c), the ELM affected area does not seem to change significantly between long and short ELMs [Schneider PPCF2014, Frassinetti NF2015]. However, due to the experimental uncertainty, the mechanism described in [Pamela EPS2014] might still be a candidate for describing the physics related to the long ELMs

Another possible mechanism that might induce the second phase of the ELM is a short transition to the L-mode, as suggested in references [Zohm NF1995 and Zhom PPCF1996]. The L-H transition has been observed to occur when the edge radial electric field shear exceeds a certain value [Sauter NF2012, Viezzer NF2013, Ryter NF2013]. The edge electric field is related to the pressure gradient normalized to the density [Viezzer PPCF2014]. If the collapse of the edge pressure gradient is large enough to reduce E_r below the critical value, a transition to the L mode might occur even if the power is above the L-H threshold. This possibility is consistent with the fact that the second ELM phase is related to a collapse of the pedestal transport barrier [Schneider PPCF2014]. Moreover, the fact that the present dataset is well above the L-H threshold might explain why the plasma returns to the H mode just 2-3ms after the crash. However, we must highlight that fast measurements of flow shear or E_r shear during ELMs have been perfomed in MAST [Kirk PPCF2005] and DIII-D [Wade PoP2005]

showing the removal of the shear layer during the ELM but without clearly observing the presence of a second ELM phase.

7. CONCLUSIONS

In conclusion, this work has discussed the ELM behavior in AUG-W without and with nitrogen seeding and has shown that the machines with metal wall (AUG-W and JET-ILW) have similar ELM phenomenology. With no nitrogen seeding, a stationary phase can be characterized by both short and long ELMs. The long ELM has a first phase that is similar to the short ELM but it is then followed by a second phase that reduces the stored energy further. The second phase is not present when the nitrogen is seeded with a sufficiently high puff rate. The disappereance of the second ELM phase is likely not related to a direct effect of the nitrogen but to the effect of the nitrogen on the pedestal top parameters and/or divertor/SOL conditions. The nitrogen seeding is also related to the increase of the temperature that leads to the collisionality reduction and hence to the increase of the energy losses of the first ELM phase. So, the nitrogen has two opposite effects on the ELM energy losses: (i) it reduces the energy losses by inducing the disappearance of the long ELMs and (ii) it increases the energy losses of the first ELM phase by reducing the collisionality.

The presence of the long ELMs is related to the pedestal temperature (or any parameter dependent on it) and/or divertor/SOL condition. The present dataset cannot clearly clarify the mechanism that drives the appeareance of the long ELMs. The experimental results suggest that the energy losses of the second phase are related to the SOL temperature, while the energy losses of the first phase to the pedestal collisionality. So, the first ELM phase and second ELM phase seem to be regulated by different mechanisms.

In terms of the power lost from the plasma and its effect on the divertor, the long ELMs are not more problematic than the short ELMs. The long ELMs higher energy losses are compensated by the longer ELM duration, so the power lost by long ELMs is not higher than for the short ELMs. Concerning the short ELMs, the increase of the nitrogen is related to the increase of energy losses and to the reduction of the ELM duration and hence to the increase of power losses. However, for the present dataset it is not possible to measure the heat flux on the divertor. It is possible that, in the divertor region, the higher power losses are, at least in part, compensated by the cooling effect of nitrogen. At present, conclusive claims on the heat flux on the divertor with nitrogen seeding are not possible.

The present results show that the ELM characteristics without and with nitrogen are similar in AUG-W and JET-ILW. In both machines it is observed that the ELMs can be characterized by two phases and that the second phase disappears at temperature and/or pressure high enough. In both machines, the first phase has energy losses that increase with nitrogen. This has been ascribed to the reduction of the pedestal collisionality.

ACKNOWLEDGEMENT

This work has been carried out within the framework of the EUROfusion Consortium and has received funding from the Euratom research and training programme 2014-2018 under grant agreement No 633053. The views and opinions expressed herein do not necessarily reflect those of the European Commission

REFERENCES

[Becoulet PPCF2001] Becoulet M et al., *Proc. 1st IAEA tech. Com. Divertor concepts (Aix-en-provence, France 2001)* Plasma Physics and Control. Fusion**.**

[Becoulet PPCF2003] Becoulet M et al., Plasma Physics and Control. Fusion **45** A93 (2003)

[Beurskens PPCF2013] Beurskens M. et al., Plasma Physics and Control. Fusion **55** 124043 (2013)

[Beurskens NF2013] M. Beurskens et al., *Nucl. Fusion* **53** 013001 (2013)

[Beursken EPS2015] Beurskens M. et al., *42th EPS Conf. on Plasma Physics*, Lisbon, Portugal (2015) P2.102

[Beurskens NF2016] M. Beurskens et al., submitted to *Nucl. Fusion*

[Bogomolov NF2016] Bogomolov A. et al., submitted to Nucl. Fusion**.**

[Boom NF2011] Boom J.E. et al., *Nucl Fusion* **51**, 103039 (2011)

[Classen RSI2012] Classen I.G.J et al. Rev. Sci. Instrum. **81** 10D929 (2010)

[Dunne EPS2015] Dunne M. et al., *42th EPS Conf. on Plasma Physics*, Lisbon, Portugal (2015) O2.109

[Dunne APS2015] Dunne M. et al., *57th Annual Meeting of the APS Division of Plasma Physics* Savannah, Georgia (2015) TO6.00011

[Eich PRL2003] Eich T et al., Phys. Rev. Lett. **91** 195003 (2003)

[Eich PPCF2005] Eich T et al., Plasma Phys. Controll. Fusion **47** 815 (2005)

[Eich JNM2011] Eich T et al., J. Nucl. Mat. **415**, S856 (2011)

[Evans PRL2004] T.E. Evans et al., Phys. Rev. Lett. **92** 235003 (2004)

[Fuchs JNM2011] Fuchs JC et al., J. Nucl. Mater. **415**, S852 (2011)

[Frassinetti NF2015] Frassinetti L. et al., Nucl. Fusion **55** 023007 (2015)

[Giroud NF2012] C. Giroud et al., Nucl. Fusion **52** 063022 (2012)

[Giroud NF2013] C. Giroud et al., Nucl. Fusion **53** 113025 (2013)

[Giroud NF2015] C. Giroud et al., Plasma Phys. Controll. Fusion **57** 035004 (2015)

[Kallenbach JNM2001] Kallenbach A. et al., J. Nucl. Mater. **290-293** 639 (2001)

[Kallenbach PPCF2010] Kallenbach A. et al., Plasma Physics and Control. Fusion **52** 055002 (2010)

[Kallenbach NF2015] Kallenbach A. et al., Nucl. Fusion **55** 053026 (2015)

[Kirk PPCF2005] Kirk A. et al., Plasma Phys. Control. Fusion **47** 315 (2005)

[Kirk NF2015] Kirk A. et al., Nucl. Fusion **55** 043011 (2015)

[Liang PRL2007] Y. Liang et al., Phys. Rev. Lett. **98** 265004 (2007)

[Loarte PPCF2002] A. Loarte et al., Plasma Phys. Control. Fusion **44** 1815 (2002)

[Loarte PPCF2003] A. Loarte et al., Plasma Phys. Control. Fusion **45** 1549 (2003)

[Maraschek EPS1998] Maraschek M et al., *25th EPS Conf. Plasma Physics, Praha, Czech Republic*, 1998 , (Ed.) Pavlo, P. (EPS, Petit-Lancy), Vol. 22C (1998), 492-495

[Matthews JNM2013] G. Matthews et al., J. Nucl. Mat. 438, S2 (2013)

[Pamela PPCF2011] S. Pamela et al., Plasma Physics and Control. Fusion **54** 054014 (2011)

[Pamela EPS2014] S. Pamela et al., *41nd EPS Conf. Plasma Physics, Berlin, Germany* (2014) P5.061

[Pitts JNM2011] R.A. Pitts et al., J. Nucl. Mater. 415, S957 (2011).

[Ryter NF2013] Ryter F et al., Nucl. Fusion **53** 113003 (2013)

[Sauter NF2012] Sauter O et al., Nucl. Fusion **52** 012001 (2012)

[Schneider PPCF2014] Schneider P. et al., Plasma Physics and Control. Fusion **56** 025011 (2014)

[Schneider PPCF2015] Schneider P. et al., Plasma Physics and Control. Fusion **57** 014029 (2015)

[Schweinzer NF2011] Schweinzer J. et al., Nucl. Fusion **51** 113003 (2011)

[Sieglin PPCF2013] Sieglin B. et al., Plasma Physics and Control. Fusion **55** 124039 (2013)

[Staebler NF1989] Staebler GM et al., Nucl. Fusion **27** 1820 (1989)

[Suttrop PRL2011] W. Suttrop et al., Phys. Rev. Lett. **106** 225004 (2011)

[Viezzer NF2013] Viezzer E et al., Nucl. Fusion **53** 053005 (2013)

[Viezzer PPCF2014] Viezzer E et al., Plasma Physics and Control. Fusion **56** 075018 (2014)

[Wade PoP2005] Wade M.R. et al., Phys. Plasmas **12**, 056120 (2005)

[Wilson EPS2001] Wilson H et al., *28th EPS Conf. on Plasma Physics*, Madeira, Portugal (2001) P3.039

[Zhitlukin JNM2007] Zhitlukin et al., J. Nucl. Matter 363, 301 (2007)

[Zohm NF1995] Zohm H et al., Nucl. Fusion **35** 543 (1995)

[Zohm PPCF1996] Zohm H et al., Plasma Physics and Control. Fusion **38** 105 (1996)

[Zohm NF2013] Zohm H et al., Nucl. Fusion **53** 073019 (2013)